


Article

Protection Effect of Ammonia on CeNbTi NH₃-SCR Catalyst from SO₂ Poisoning

Yang Gao ^{1,†}, Li Cao ^{1,†}, Xiaodong Wu ^{1,*} , Xu Zhang ¹, Ziran Ma ², Rui Ran ¹, Zhichun Si ³, Duan Weng ^{1,3,*} and Baodong Wang ²

¹ The Key Laboratory of Advanced Materials of Ministry of Education, School of Materials Science and Engineering, Tsinghua University, Beijing 100084, China

² National Institute of Clean-and-Low-Carbon Energy (NICE), Beijing 102209, China

³ Advanced Materials Institute, Graduate School at Shenzhen, Tsinghua University, Shenzhen 518055, China

* Correspondence: wuxiaodong@mail.tsinghua.edu.cn (X.W.); duanweng@tsinghua.edu.cn (D.W.)

† These authors contributed equally to this work.

Abstract: CeNbTi catalyst was poisoned in different sulfur poisoning atmospheres at 300 °C for 6 h and then was evaluated for selective catalytic reduction (SCR) of NO_x with NH₃. The catalyst deactivation upon SO₂ exposure was effectively inhibited in the presence of NH₃. Temperature-programmed decomposition (TPD) analyses were applied to identify deposit species on the poisoned catalysts by comparison with several groups of reference samples. Diffuse reflectance infrared Fourier transform spectroscopy (DRIFTS) over CeNbTi catalysts with different poisoning pretreatments and gas purging sequences were designed to investigate the roles of NH₃ in the removal of surface sulfites and sulfates. More ammonium sulfates including ammonium bisulfate and ammonium cerium sulfate were generated instead of inert cerium sulfate in these conditions. The mechanisms about the formation and transformation of surface deposits upon sulfur poisoning w/wo NH₃ were explored, which provided a basis for developing Ce-based mixed oxides as SCR catalysts for stationary sources.

Keywords: ceria; SCR; sulfur; NH₃; TPD; DRIFTS; deposit



Citation: Gao, Y.; Cao, L.; Wu, X.; Zhang, X.; Ma, Z.; Ran, R.; Si, Z.; Weng, D.; Wang, B. Protection Effect of Ammonia on CeNbTi NH₃-SCR Catalyst from SO₂ Poisoning. *Catalysts* **2022**, *12*, 1430. <https://doi.org/10.3390/catal12111430>

Academic Editor: Rufino Navarro Yerga

Received: 18 October 2022

Accepted: 11 November 2022

Published: 14 November 2022

Publisher's Note: MDPI stays neutral with regard to jurisdictional claims in published maps and institutional affiliations.



Copyright: © 2022 by the authors. Licensee MDPI, Basel, Switzerland. This article is an open access article distributed under the terms and conditions of the Creative Commons Attribution (CC BY) license (<https://creativecommons.org/licenses/by/4.0/>).

1. Introduction

Over the past decades nitrogen oxides (NO_x) that are produced from mobile and stationary sources have led to many environment problems [1]. The selective catalytic reduction (SCR) of NO_x using ammonia as the reductant is one of the most promising deNO_x technologies [2]. Ceria-based catalysts have attracted plenty of interest due to some advantageous features including high NO_x conversion, nontoxicity, and low cost [3–6]. Recently, the activity and hydrothermal stability of ceria-based catalysts have been improved by inducing WO₃ and SnO₂ as a promoter, realizing over 90% NO_x conversion at 300–550 °C after hydrothermal-aging at 1000 °C, as reported by He et al. [7,8]. This means the application scenarios of ceria-based catalysts are broadened, such as used downstream of the diesel particulate filter (DPF). However, in typical application scenarios, especially coal-fired power plants or the aftertreatment system of marine diesel engines, the effluent gases always contain a certain concentration of SO₂. Thus, SO₂ resistance is one of the most important characteristics of SCR catalysts. The deposition of cerium sulfates and ammonium bisulfate has been recognized as the main factor of deactivation of ceria-based catalysts. The deactivation of these catalysts in the presence of SO₂ is sensitive to reaction temperatures. Zhang et al. [9] reported that with the increase of reaction temperature from 180 to 300 °C, the content of cerium sulfates increased significantly, accompanied with the decreased deposition of ammonium sulfates/bisulfates. Zhang et al. [10] found that the sulfation process was gradually worsened with raising the treating temperature, and the sulfate species over CeO₂ changed from surface sulfates to bulk-like ones, and then to bulk

ones. These studies indicate that different sulfur species are formed on ceria-based catalysts at different temperature ranges, which affect NH_3 -SCR activity significantly.

In addition to reaction temperatures, other gases, especially ammonia, influence the type of sulfur species that is formed during SO_2 poisoning. Research on the effects of ammonia on SO_2 poisoning have been focused on Cu-CHA catalysts [11–13]. For example, as investigated by Wijayanti et al. [11,12], ammonium-sulfur species formed over Cu-SSZ-13 during sulfur poisoning under SCR conditions at 300 °C, reducing the availability of copper sites for the redox SCR cycle due to the site-blocking effect of the deposits [12]. Wang et al. [13] found that copper sulfate was present in all the Cu/SAPO-34 samples that were sulfated at various temperatures, whereas ammonia sulfate was only found over the sample at 250 °C. They suggested that both copper sulfate and ammonia sulfate species decrease the SCR reaction rate of the Cu/SAPO-34 catalyst by reducing the number of Cu^{2+} sites. Moreover, Jangjou et al. [14] found that ammonia can drive sulfur from a more thermodynamically copper sulfate to less stable ammonium sulfate over Cu/SAPO-34 catalysts. The results showed that ammonium affected the types of sulfur-containing species. This appears favorable, as NH_3 can react with pre-adsorbed sulfur on the catalyst to form ammonium-sulfur species, which decomposes at lower temperatures in comparison to the other sulfate forms.

Besides, similar phenomena have also been observed over Fe-W and Nb-V/Ce catalysts in recent studies [15,16], that the introduction of NH_3 in the sulfation process at 300 °C dramatically reduced the formation of surface metal sulfate species. $\text{Fe}_2(\text{SO}_4)_3$ can decompose in NH_3 atmosphere at approximately 220 °C, helping reduce sulfate deposit on the catalyst [15]. The NH_3 -SCR performances of metal oxide catalysts (such as $\gamma\text{-Fe}_2\text{O}_3$, CeO_2 , and $\gamma\text{-MnO}_2$) in a sulfur-containing atmosphere were closely related to the difference in the deposition/decomposition ability of the formed sulfate species as reported by An et al. [17]. Adsorbed NH_3 and H_2O can promote the decomposition of metal sulfate $\text{Me}(\text{SO}_4)_y$, proven by temperature-programmed surface reaction (TPSR) of NH_3 .

Despite the above studies, the SO_2 poisoning over ceria-based catalysts in an SCR environment, to our knowledge, has not been comprehensively studied. Different from Cu-CHA, ceria-based catalysts tend to deactivate more quickly in sulfur poisoning due to the formation of cerium sulfate. This may have a positive effect on the activity if the formation of cerium sulfate can be inhibited in the NH_3 -containing atmospheres. Therefore, sulfur poisoning in different atmospheres is worth studying for ceria-based catalysts. In our previous work [18,19], the addition of niobium on CeWTi catalyst resulted in high NO_x conversion in a wide temperature window and significantly improved sulfur resistance at low and medium temperatures. In this work, CeNbTi was chosen as a typical ceria-based oxides catalyst, and 300 °C was chosen as a typical temperature for sulfur poisoning of SCR catalysts. The sulfur poisoning mechanism of CeNbTi catalyst in an SCR environment and specifically the role of NH_3 were explored.

2. Experimental

2.1. Catalyst Preparation

CeNbTi catalyst was prepared by a co-precipitation method. $\text{C}_{12}\text{H}_7\text{NbO}_{24}$ (Aladdin, China) and $\text{Ce}(\text{NO}_3)_3 \cdot 6\text{H}_2\text{O}$ (Aladdin) were dissolved in deionized water with a Nb_2O_5 : CeO_2 mass ratio of 2:1. The precursors were mixed with commercial TiO_2 powders (DT51, Cristal, Saudi Arabia) in deionized water according to a $(\text{Nb}_2\text{O}_5 + \text{CeO}_2)$: TiO_2 molar ratio of 3:7. Diluted ammonium hydroxide (Beijing Chem., Beijing, China) was then added in the mixed solution as a precipitating agent under vigorous stirring. The obtained precipitate was dried at 110 °C overnight and calcined in a muffle furnace at 600 °C for 5 h. The loading of CeO_2 and Nb_2O_5 are 12 wt.% and 22 wt.%, respectively.

The poisoned catalysts were obtained by treating the as-received CeNbTi in a gas flow consisting of 500 ppm NO (when used), 500 ppm NH_3 (when used), 200 ppm SO_2 (when used), 5% H_2O (when used), 5% O_2 , and balanced N_2 at 300 °C for 6 h.

For reference, the deposited catalysts were prepared by an incipient wetness impregnation method. Ammonium sulfite (Aladdin), ammonium hydrogen sulfate (Aladdin), cerium sulfate (Aladdin), and ammonium cerium sulfate (Aladdin) were impregnated on the CeNbTi catalyst with a nominal loading of 2 wt.%. The aqueous solution was added dropwise to the catalyst powders. The mixture was dried at 80 °C for 12 h, and the obtained samples were denoted as (NH₄)₂SO₃/CeNbTi, NH₄H₂SO₄/CeNbTi, Ce(SO₄)₂/CeNbTi, and (NH₄)₄Ce(SO₄)₄/CeNbTi, respectively.

2.2. Activity Measurement

The NH₃-SCR activity measurement was carried out in a fixed bed reactor with powder catalyst (200 mg, 40–60 mesh). The reaction gas mixture consisted of 500 ppm NO, 500 ppm NH₃, 5% O₂, 5% H₂O, and N₂ in balance. The gas hourly space velocity (GHSV) was 80,000 h⁻¹ and the reaction temperature was set at 300 °C. The NO_x (NO, NO₂, and N₂O) concentrations in the outlet gases were measured by a Nicolet 380 infrared (IR) spectrometer (Thermo Fisher, Waltham, MA, USA). The NO_x conversion was calculated as follows:

$$\text{NO}_x \text{ conversion (\%)} = \frac{[\text{NO}]_{\text{in}} + [\text{NO}_2]_{\text{in}} - [\text{NO}]_{\text{out}} - [\text{NO}_2]_{\text{out}}}{[\text{NO}]_{\text{in}} + [\text{NO}_2]_{\text{in}}} \times 100 \quad (1)$$

2.3. Catalyst Characterization

Nitrogen adsorption isotherms were measured on a JW-BK200(JWGB, China) instrument. All the samples were degassed at 220 °C for 1 h before the nitrogen adsorption measurements. The Brunner–Emmett–Teller (BET) surface area was calculated by a multi-point BET method.

Temperature-programmed decomposition (TPD) analyses were performed on an MKS 2030 Fourier transform infrared (FT-IR) gas analyzer (MKS Instruments, USA). A total of 100 mg sample was pretreated in N₂ at 100 °C for 30 min. Then, the sample was ramped to 1000 °C at a rate of 10 °C/min in N₂.

In situ diffuse reflectance infrared Fourier transform spectroscopy (DRIFTS) was performed on a Nicolet 6700 IR spectrometer (Thermo Fisher). The spectra were calculated by the Kubelka–Munk function. The reaction atmosphere consisted of 200/500 ppm NH₃ (when used), 100/200 ppm SO₂ (when used), 5% O₂, and N₂ in balance. The catalyst in a diffuse reflectance IR cell was pretreated by N₂ (100 mL/min) at 500 °C for 30 min to remove traces of organic residues. Then, the sample was cooled down to 100 °C. Afterward, the samples were purged with the reaction atmosphere and the spectra were collected as a function of time.

3. Results

3.1. NH₃-SCR Activity

The NO_x conversions of the used and poisoned catalysts were obtained from the isothermal activity test at 300 °C and the results are shown in Figure 1. After running in a standard NH₃-SCR condition for 6 h, the used CeNbTi catalyst still exhibited high SCR activity, with a temperature window of 195–420 °C in which the NO_x conversion exceeded 80% (Figure S1). When only SO₂ and O₂ are applied for a sulfur poisoning test, the catalyst is deactivated severely with the NO_x conversion declining sharply to 62%. Such a poisoning effect is maintained in the presence of water. Nevertheless, the runnings in NH₃-containing atmospheres prevent the catalyst deactivation to a great extent, and these poisoned catalysts show ca. 90% NO_x conversion. Again, the influence of water can be omitted. To judge the role of NO, it was removed from the treating atmosphere and the NO_x conversion of the obtained catalyst increased slightly from 88% to 91%. A similar negligible role of H₂O can also be observed. All these demonstrate that ammonia is responsible for the greatly improved sulfur resistance of the ceria-based catalyst.

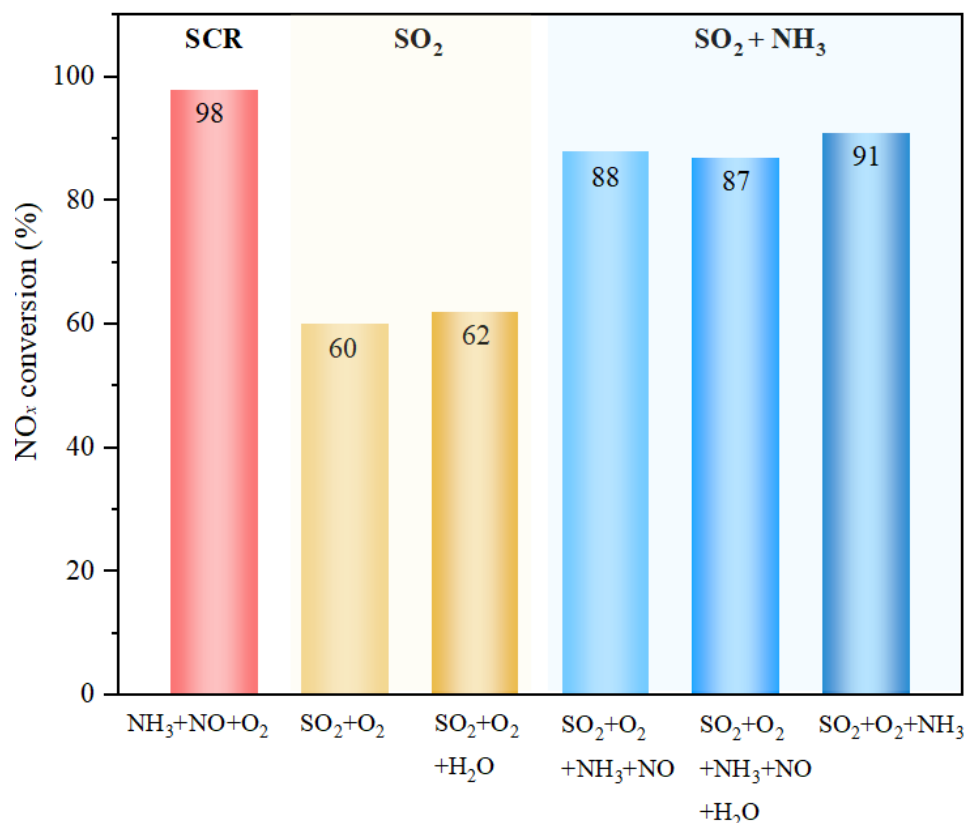


Figure 1. SCR activity of the treated CeNbTi catalysts. Reaction conditions: 500 ppm NO, 500 ppm NH₃, 5% O₂, 5% H₂O, N₂ in balance, 300 °C, and GHSV = 80,000 h⁻¹.

3.2. TPD Analyses

3.2.1. Identification of Surface Deposits

To identify the deposits on the poisoned catalysts, the TPD experiments were performed in N₂. Almost no NO_x (including NO, NO₂, and N₂O) were observed within the whole temperature range (not shown), indicating their poor adsorption when competing with sulfur oxides. Figure 2 shows the evolution of SO₂ and NH₃ signals during the TPD processes. The NH₃ and SO₂ desorption were estimated by peak fitting and the results are summarized in Table 1. Since the sulfur poisoning tests were performed at 300 °C, the NH₃ signal also starts at this temperature in Figure 2a. The NH₃ release (16 μmol/g) for the catalyst that was treated in a simple SCR condition (without SO₂) is derived from desorption of ammonia that is adsorbed at surface acid sites. The ammonia desorption is doubled in the SO₂-containing treating atmospheres. According to the reports of Xu et al. [9] and Song et al. [20], the increased ammonia can be related to the formation of ammonium sulfates including ammonium bisulfate, ammonium sulfate, and ammonium cerium sulfate. The presence of H₂O or NO does not affect the ammonium adsorption on the catalyst upon the sulfur poisoning treatments. Since the specific surface areas of catalysts almost have no changes with or without NH₃-containing SO₂ poisoning atmosphere and the maximal amount of NH₄HSO₄ (about 17 μmol/g) is much smaller than that of metal sulfates and ammonium metal sulfates, the physical poisoning (covering effect) of the deposited NH₄HSO₄ should not be the main factor to deactivate the catalyst.

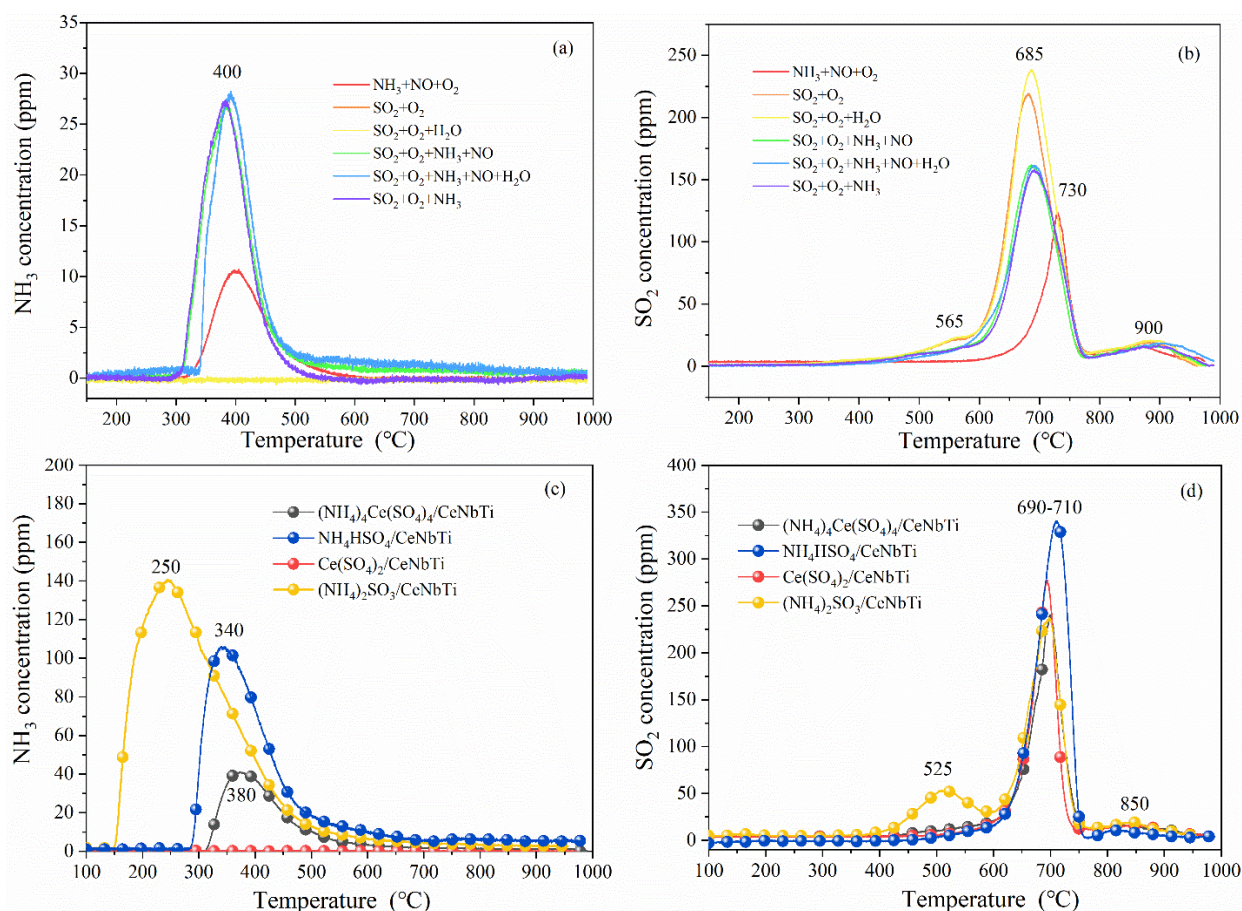


Figure 2. TPD curves of (a,c) NH₃ and (b,d) SO₂ over the treated (a,b) and deposited (c,d) catalysts.

Table 1. Amounts of NH₃ and SO₂ that were released from the treated catalysts during the TPD tests.

Sample	S _{BET} (m ² /g)	NH ₃ (μmol/g)	SO ₂ (μmol/g)				Deposit *
			Peak Temperature (°C)				
			565	685	730	900	
NH ₃ + NO + O ₂	113	16	0	0	98	34	-
SO ₂ + O ₂	85	0	35	185	98	34	220
SO ₂ + O ₂ + H ₂ O	87	0	35	212	98	38	247
SO ₂ + O ₂ + NH ₃ + NO	93	35	17	131	98	37	148
SO ₂ + O ₂ + NH ₃ + NO + H ₂ O	86	33	15	129	98	32	144
SO ₂ + O ₂ + NH ₃	89	34	17	125	98	32	142

* Estimated by the sum of peaks at 565 and 685 °C.

Compared with NH₃, the SO₂ signal appears at much higher temperatures (450–1000 °C) in Figure 2b. Interestingly, there are two SO₂ peaks over the catalyst that was treated in the simple SCR condition without SO₂. The distinct SO₂ peak centered at 730 °C with a shoulder at 900 °C is associated with the decomposition of titanium sulfates in the original material [18,21,22]. After sulfur poisoning, the major peak shifts towards a lower temperature (685 °C) and another small peak appears at 565 °C. According to the previous studies [23,24], the low-temperature peak is ascribed to the decomposition of metal sulfites. The overlapped peak at 685 °C is attributed to the decomposition of ammonium sulfates and cerium sulfates [25,26]. When ammonia is added into the poisoning atmosphere, both the SO₂ peaks at 565 and 685 °C decrease in intensity significantly. As listed in Table 1, about two thirds of sulfites and about one third of sulfate deposits are reduced on those catalysts.

To further verify the deposits on the treated catalysts, one group of reference samples was prepared and their TPD curves are shown in Figure 2c,d. Among these samples, $(\text{NH}_4)_2\text{SO}_3$, NH_4HSO_4 , $\text{Ce}(\text{SO}_4)_2$, and $(\text{NH}_4)_4\text{Ce}(\text{SO}_4)_4$ were chosen as the representatives of ammonium sulfites, ammonium bisulfates, cerium sulfates, and ammonium ceria sulfates, respectively. The NH_3 desorption occurs at a much lower temperature (around 250 °C) over $(\text{NH}_4)_2\text{SO}_3/\text{CeNbTi}$. Comparatively, the NH_3 desorption peak appears at 340 and 380 °C for the NH_4HSO_4 and $(\text{NH}_4)_4\text{Ce}(\text{SO}_4)_4$ impregnated catalysts, respectively, which are close to those (400 °C) over the catalysts that were poisoned in the NH_3 -containing atmospheres Figure 2a.

As shown in Figure 2d, a small SO_2 desorption peak at 525 °C is only found over $(\text{NH}_4)_2\text{SO}_3/\text{CeNbTi}$, indicating the origin of the 565 °C peak in Figure 2b. It is interesting that a distinct peak at 700 °C is also observed for this sample. One possible explanation is the re-adsorption of SO_2 from sulfite decomposition with ceria acting as strong basic sites, which releases at higher temperatures. Another possibility that cannot be excluded is that sulfites may be readily oxidized to sulfates by active oxygen in ceria during the impregnation and TPD processes. Similar phenomena about delayed release of SO_2 have been observed over many catalysts including VTi, VWTi, and Cu-SSZ-13 [26–28]. All the impregnated sulfates show a similar SO_2 desorption peak at 600–750 °C. Therefore, it is difficult to identify specific sulfates from the 685 °C desorption peaks in Figure 2b in this way. Nevertheless, some important information can still be deduced. Considering the fact that almost only cerium sulfates ($\text{Ce}(\text{SO}_4)_2$ and $\text{Ce}_2(\text{SO}_4)_3$) are generated in the poisoning atmospheres without NH_3 and the total SO_2 desorption declines over the $\text{SO}_2 + \text{NH}_3$ co-treated catalysts (Figure 2b), the additional NH_3 release over the latter catalysts (Figure 2a) should be ascribed to the decomposition of ammonium sulfates such as NH_4HSO_4 and $(\text{NH}_4)_4\text{Ce}(\text{SO}_4)_4$. All these indicate that the formation of cerium sulfates is inhibited to a large extent in the presence of NH_3 .

3.2.2. Effect of Ammonia on Surface Deposits

To investigate the mechanism of NH_3 addition on the sulfur resistance of CeNbTi catalyst, several experiments were performed to characterize structural changes after the durability tests. No obvious differences were observed in the XRD patterns (Figure S2) of the fresh and poisoned catalysts. Only the characteristic peaks of anatase TiO_2 are observed, and those of ceria, niobia, or sulfates do not appear due to their low crystallinity. In order to further identify the deposits on the poisoned catalyst, another group of reference samples was prepared by treating CeNbTi catalyst with $\text{SO}_2 + \text{O}_2$ and NH_3 in different sequences before TPD experiments. As shown in Figure 3, a short-time (30 min) pretreatment in $\text{SO}_2 + \text{O}_2$ resulted in similar TPD curves of NH_3 and SO_2 as those for a much longer period (6 h). The sulfite-related SO_2 desorption peak of the former catalyst is even stronger than that in Figure 3b, indicating the transformation of sulfites to sulfates proceeded with time-on-stream. After that, NH_3 alone was introduced to react with the sulfates/sulfites on the $\text{SO}_2 + \text{O}_2$ pretreated catalyst and then the TPD measurement was performed. Here, the sulfite-related peak almost diminishes due to the formation and following decomposition of ammonium sulfite. As shown by the TG/DSC curves in Figure S3, ammonium sulfite decomposes easily even at temperatures below 120 °C. It implies that once it was formed by a reaction of metal sulfites with the introduced ammonia, ammonia sulfite would decompose subsequently during the pretreatment. As a result, few metal sulfites exist on the catalyst after NH_3 purging (Figure 3b). Meanwhile, a small NH_3 desorption peak occurs at 400 °C (Figure 3a), assigned to the decomposition of ammonium sulfates and chemisorbed ammonia on the surface acid sites.

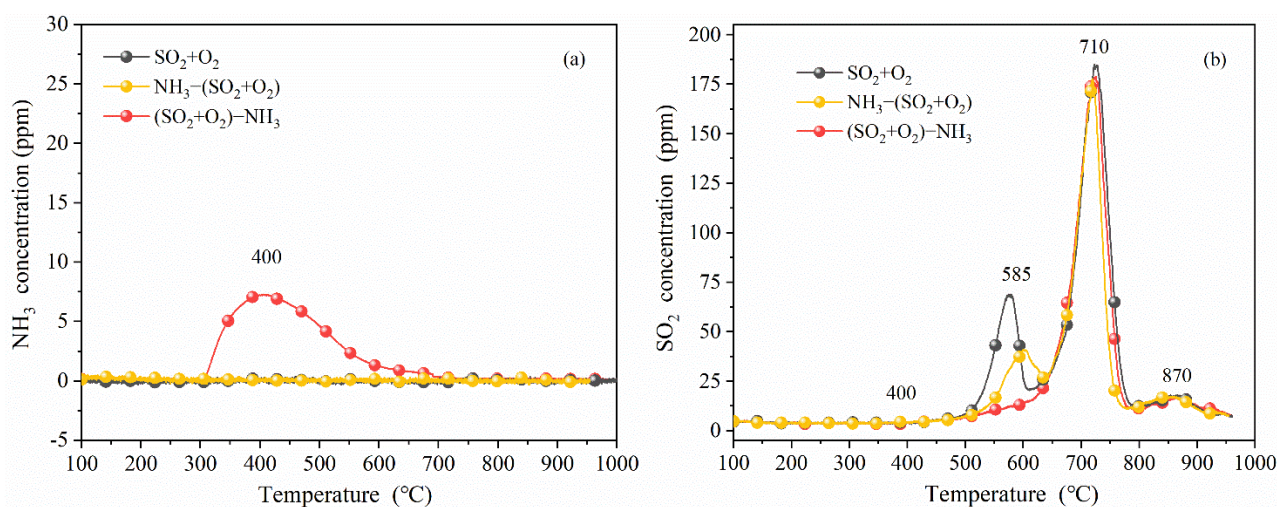


Figure 3. TPD curves of (a) NH_3 and (b) SO_2 over the catalyst that was pretreated in $\text{SO}_2 + \text{O}_2$ and NH_3 in different sequences.

Then, a reverse sequence was adopted for purging gases. The catalyst was first pretreated in NH_3 for 30 min, aiming to saturate NH_3 adsorption, and then the feeding gas was switched to $\text{SO}_2 + \text{O}_2$. It is interesting to find that the sulfite-related SO_2 peak significantly decreases in intensity and almost no NH_3 desorbs. In this case, the adsorbed NH_3 is firstly consumed by gaseous SO_2 via forming ammonium sulfite and subsequent decomposition, as well as driven by competitive adsorption of SO_x . Then, the continuous passing with $\text{SO}_2 + \text{O}_2$ produces ceria-based sulfite and sulfate species. It is noted that the sulfate-related SO_2 desorption peak decreases slightly in intensity after purging with NH_3 (Figure 3b). It demonstrates that NH_3 can remove surface sulfites but release the deposited sulfates to a small extent within the limited time. Thus, the reduced sulfate deposits in the presence of NH_3 (Figure 3b) should be ascribed to a great extent to other factors such as competitive adsorption between NH_3 and SO_2 .

3.3. Infrared Studies

3.3.1. Surface Groups Identification

Ex situ IR spectra of the treated CeNbTi catalysts were compared with reference samples to determine surface deposit species. As shown in Figure 4a, four main bands are found in the spectrum of ammonium sulfite. The bands at 1183, 1027, and 930 cm^{-1} are assigned to sulfite species [29], and the one at 1502 cm^{-1} is assigned to NH_4^+ on Brønsted acid sites [30]. In the case of ammonium hydrogen sulfate (Figure 4b), the band at 1478 cm^{-1} is attributed to asymmetric bending vibrations of NH_4^+ and the bands at 1326 and 1260 cm^{-1} are assigned to the S=O vibration absorption singles of HSO_4^- [31]. For cerium sulfate (Figure 4c), the bands at 1367 and 1300 cm^{-1} are related to the asymmetric stretching frequencies of O=S=O species [32]. The band at 1660 cm^{-1} is assigned to O-H stretching modes from the reaction between SO_2 and surface hydroxyl groups [33,34]. As for ammonium cerium sulfate, five characteristic bands are observed in Figure 4d. The distinct band at 1275 cm^{-1} with a shoulder at 1200 cm^{-1} is ascribed to bidentate sulfate species [35]. The band at 1067 cm^{-1} is attributed to the S-O ν_3 vibrations of Ce-bonded bidentate SO_4^{2-} in C_{2v} symmetry [36]. The bands at 1606 and 1468 cm^{-1} are assigned to the NH_4^+ on Brønsted acid sites [37].

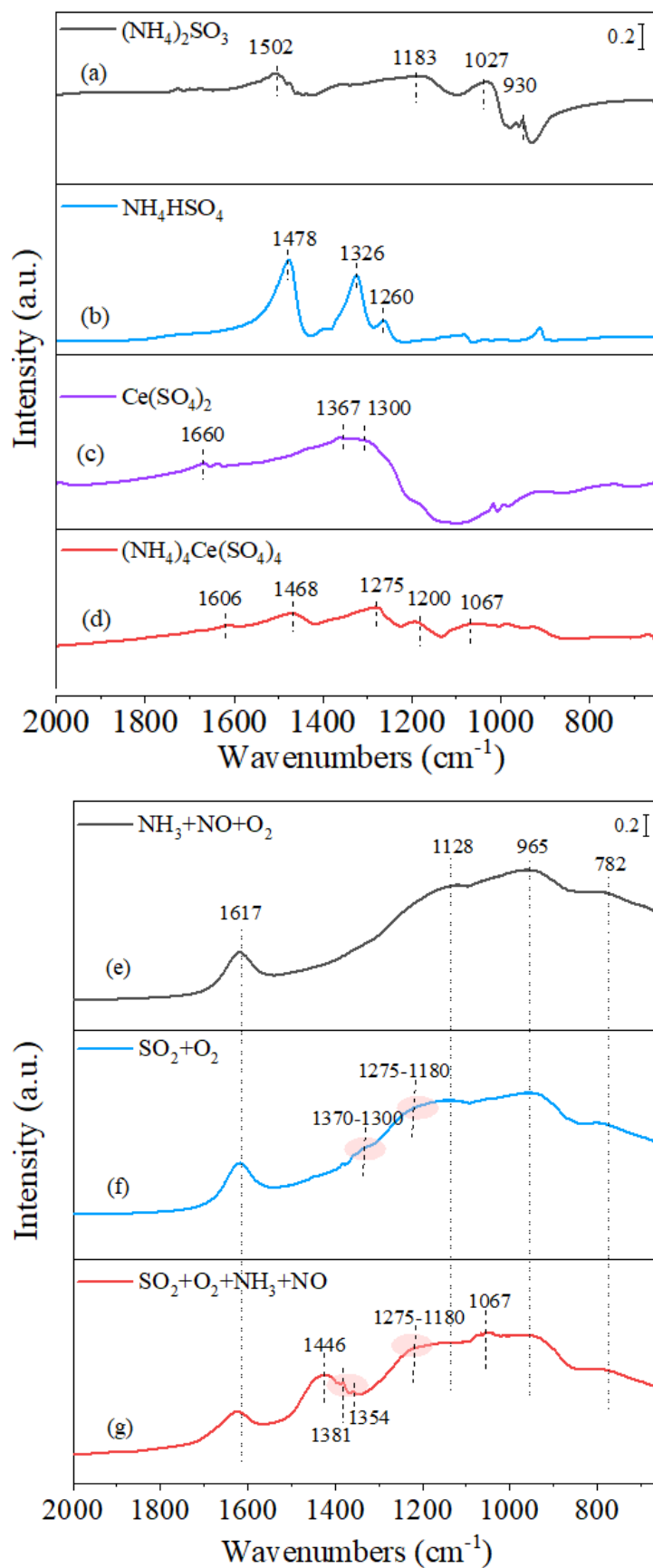


Figure 4. IR spectra of (a–d) reference samples and (e–g) treated CeNbTi catalysts.

The IR spectrum of the CeNbTi that was treated in a simple SCR condition is shown in Figure 4e as the background. The band at 1617 cm^{-1} is assigned to adsorb H_2O from the reaction between SO_2 and surface hydroxyl groups [33]. The band at 965 cm^{-1} is attributed to characteristic vibrations of $\text{Nb}=\text{O}$ bond in surface NbO_x species [23] and the one at 1128 cm^{-1} is due to modes of $\text{Nb}-\text{O}-\text{Nb}$ stretching vibration [38,39]. The stretching modes of $\text{Ce}-\text{O}-\text{Ce}$ bands generally results in a band at 729 cm^{-1} [34], which shifts to 782 cm^{-1} due to interacting with Nb_2O_5 [38]. As for the spectrum that was collected over the catalyst upon exposure to $\text{SO}_2 + \text{O}_2$ (Figure 4f), the sulfate-related bands can be observed. There are two broad bands ranging at $1370\text{--}1300$ and $1275\text{--}1180\text{ cm}^{-1}$ that are ascribed to the asymmetric stretching frequencies of the $\text{O}=\text{S}=\text{O}$ bond and $\text{S}-\text{O}$ bond of bidentate sulfate species, respectively. $\text{SO}_2 + \text{O}_2 + \text{NH}_3 + \text{NO}$ was chosen as a representative of three NH_3 -containing poisoning atmospheres. As shown in Figure 4g, the spectrum of the obtained catalyst exhibits a characteristic band at 1446 cm^{-1} . It is assigned to the asymmetric bending vibrations of ionic NH_4^+ that is bound to Brønsted acid sites that are provided by surface sulfates (i.e., NH_4HSO_4 and $(\text{NH}_4)_4\text{Ce}(\text{SO}_4)_2$). Considering the similar intensities of the 1478 and 1326 cm^{-1} bands for NH_4HSO_4 (Figure 4b), the extra intensified band at 1446 cm^{-1} may mean the formation of ammonium cerium sulfate to a great extent. Another evidence is the band at 1067 cm^{-1} that is attributed to Ce-bonded bidentate sulfates. The broad band at $1275\text{--}1180\text{ cm}^{-1}$ may come from HSO_4^- , CeSO_4 , and $(\text{NH}_4)_4\text{Ce}(\text{SO}_4)_4$. Other adsorption bands of sulfates at 1381 and 1354 cm^{-1} are attributed to asymmetric stretching frequencies of $\text{O}=\text{S}=\text{O}$ species that are related to the formation of $\text{Ce}(\text{SO}_4)_2$.

3.3.2. In Situ $\text{SO}_2 + \text{O}_2$ Adsorption

Figure 5a shows the DRIFT spectra of adsorbed species over CeNbTi catalyst in a $\text{SO}_2 + \text{O}_2$ flow at $100\text{ }^\circ\text{C}$ as a function of time. As the signals that were obtained by performing the DRIFTS experiments at $300\text{ }^\circ\text{C}$ are much weaker, the adsorption of reactants and products becomes more significant by reducing the operating temperature to $100\text{ }^\circ\text{C}$. Hereby, the sulfur poisoning and ammonium protecting effects are amplified, although the specific mechanisms may be somewhat different at two temperatures. The band at 1268 cm^{-1} is assigned to bidentate sulfates [35], while several small features at 1180 , 1024 , and 925 cm^{-1} are attributed to sulfite species that are associated with different adsorption sites [33]. The band at 1086 cm^{-1} could be assigned to ν_3 vibrations of bidentate SO_4^{2-} in C_{2v} symmetry [36], while those at 1383 and 1300 cm^{-1} could be attributed to the asymmetric stretching frequencies of $\text{O}=\text{S}=\text{O}$ species for sulfates that were adsorbed on metal oxides [32]. The band at 1430 cm^{-1} is attributed to the formed $\text{S}-\text{OH}$ from the reaction between SO_2 and metal cations [18]. The band at 1630 cm^{-1} is assigned to $\text{O}-\text{H}$ stretching modes from the reaction between SO_2 and surface hydroxyl groups [33,34]. All these bands increase sharply in intensity with time, indicating the deposition of a large amount of sulfite/sulfate species on CeNbTi catalyst upon sulfur poisoning.

3.3.3. In Situ Surface Reaction between Ad-Species and NH_3/SO_2

As mentioned above, fewer sulfates and sulfites formed when SO_2 poisoning tests were performed in the NH_3 -containing atmospheres. In order to understand how NH_3 affects the adsorbed sulfate/sulfite species, DRIFTS was performed to characterize the evolution of surface species on the $\text{SO}_2 + \text{O}_2$ pretreated catalyst upon exposure to NH_3 and the results are shown in Figure 5b. The sulfate bands (1428 , 1383 , 1300 , 1268 , and 1086 cm^{-1}) and sulfite bands (1024 and 925 cm^{-1}) were observed for the pretreated catalyst. After purging with NH_3 for 30 min, a new band appears at 1676 cm^{-1} , assigned to NH_4^+ species that are bound to Brønsted acid sites [38,40]. Meanwhile, one band that was assigned to sulfate species shifts from 1430 to 1452 cm^{-1} . The regular IR spectrum of ammonium bisulfate and ammonium cerium sulfate shows a NH_4^+ characteristic band at 1478 (Figure 4b) and 1468 cm^{-1} (Figure 4c), respectively. Both the asymmetric bending vibrations of NH_4^+ and the formed $\text{S}-\text{OH}$ from metal sulfates contribute to this band.

Thus, it implies the generation of ammonium cerium sulfate and ammonium bisulfate after the introduction of NH_3 . Meanwhile, the metal sulfate bands (1383 and 1300 cm^{-1}) disappear finally, suggesting the transformation of $\text{Ce}(\text{SO}_4)_2$ to $(\text{NH}_4)_4\text{Ce}(\text{SO}_4)_4$ since NH_4^+ bonding with SO_4^{2-} consumes $\text{O}=\text{S}=\text{O}$ in $\text{Ce}(\text{SO}_4)_2$ [41], and the latter species decomposes subsequently (Figure S4).

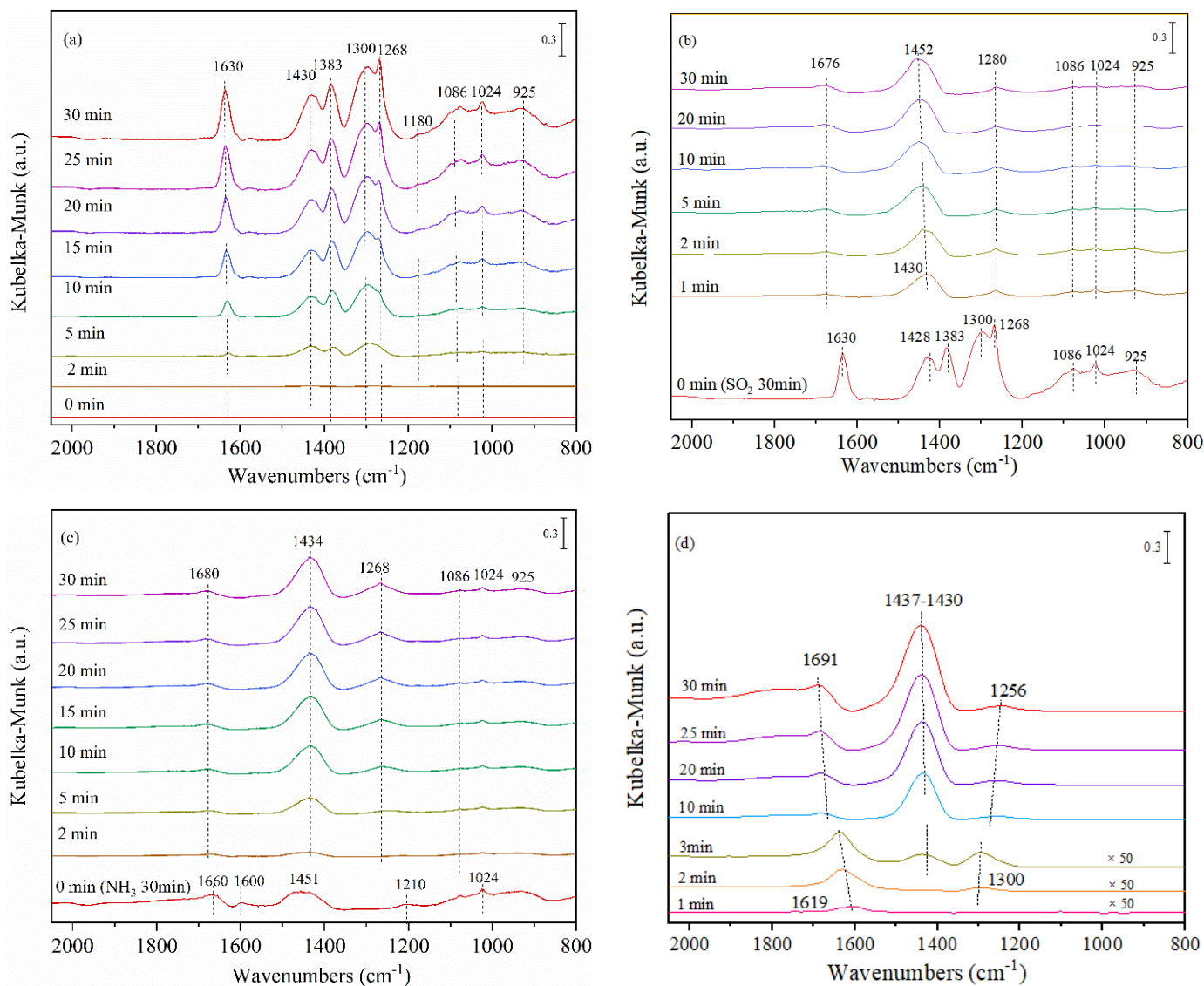


Figure 5. DRIFT spectra of (a) the catalyst exposed to $\text{SO}_2 + \text{O}_2$ as a function of time, (b) the $\text{SO}_2 + \text{O}_2$ pretreated catalyst exposed to NH_3 , (c) the NH_3 pretreated catalyst exposed to $\text{SO}_2 + \text{O}_2$, and (d) the catalyst exposed to $\text{NH}_3 + \text{SO}_2 + \text{O}_2$ at $100\text{ }^\circ\text{C}$ as a function of time.

A reverse DRIFT spectroscopy was also performed to explore the evolution of surface species on the NH_3 pretreated catalyst upon exposure to $\text{SO}_2 + \text{O}_2$. As shown in Figure 4c, the Brønsted acid site-related bands (1660 and 1451 cm^{-1}) and Lewis acid site-related bands (1600 , 1210 , and 1024 cm^{-1}) are observed initially for the pretreated catalyst [10,34,42,43]. After the introduction of SO_2 , the sulfate-related bands (1434 , 1266 , and 1068 cm^{-1}) form with time-on-stream. Importantly, the bands at 1383 and 1300 cm^{-1} that were attributed to CeSO_4 can hardly be observed, illustrating that introduced SO_x prefers to react with adsorbed NH_3 to form NH_4HSO_4 and $(\text{NH}_4)_4\text{Ce}(\text{SO}_4)_4$. Meanwhile, the sulfite-related bands at 1022 and 925 cm^{-1} appear slowly. By comparison with the case of the as-received catalyst (Figure 5c), it indicates that the adsorbed ammonia reduces the formation of metal

sulfates effectively. That is, the competitive adsorption between NH_3 and SO_2 would improve the sulfur resistance of the catalyst greatly.

Furthermore, in order to judge the discrepancy of NH_3 and SO_2 adsorption capacity over the CeNbTi catalyst, a competitive adsorption test was performed in a gas stream containing 200 ppm NH_3 , 200 ppm SO_2 , and 5% O_2 . At the initial stage (1 min) in Figure 5d, NH_3 is preferentially adsorbed on Brønsted acid sites with the symmetric bending vibrations of NH_4^+ at 1618 cm^{-1} , and then (2 min) the signal of S-O bond in SO_4^{2-} appears at 1300 cm^{-1} . After that (3 min), overlapped signals of the asymmetric bending vibrations of adsorbed NH_4^+ and the S-OH vibrations of SO_4^{2-} appear at 1430 cm^{-1} . The vibration signals of NH_4^+ and SO_4^{2-} show a blue shift to a higher wavenumber and a red shift to lower wavenumber, respectively. This was derived from more NH_3 adsorption forming $\text{NH}_4^+[\text{NH}_3]_n$ structure [44], O-H from the reaction between SO_2 and surface hydroxyl groups, and SO_4^{2-} influenced by ammonia. These results demonstrate that the ammonia co-adsorbs on the CeNbTi catalyst with SO_2 and could promote metal sulfates species transforming to ammonium sulfate-type and ammonium metal sulfate-type species.

4. Discussion

Intrinsically, NH_3 as an alkaline gas can facilitate SO_2 adsorption on ceria-based catalysts by the formation of ammonium sulfate-type species. Figure 6 shows the evolution of the typical sulfate bands ($1300\text{--}1256\text{ cm}^{-1}$) and sulfite band (925 cm^{-1}) over the CeNbTi catalyst that was treated by different poisoning procedures that were derived from Figure 5a,c,d, respectively. The peak areas of these bands were integrated and drawn as a function of time. In a simplified atmosphere ($\text{SO}_2 + \text{O}_2$), the sulfate bands increase in intensity continuously (Figure 6a), with cerium sulfate as the main product (Equation (2)), proven by the infrared spectra in Figures 4f and 5a. It also correlates with the TG results (Table 1) that after the treatment in $\text{SO}_2 + \text{O}_2$ for 6 h, about 13% of CeO_2 transforms to cerium sulfate by assuming cerium sulfate as the dominating metal sulfate. Similarly, the sulfite band also obviously increases in intensity (Figure 6b), with the transformation of about 3% of CeO_2 to cerium sulfites.

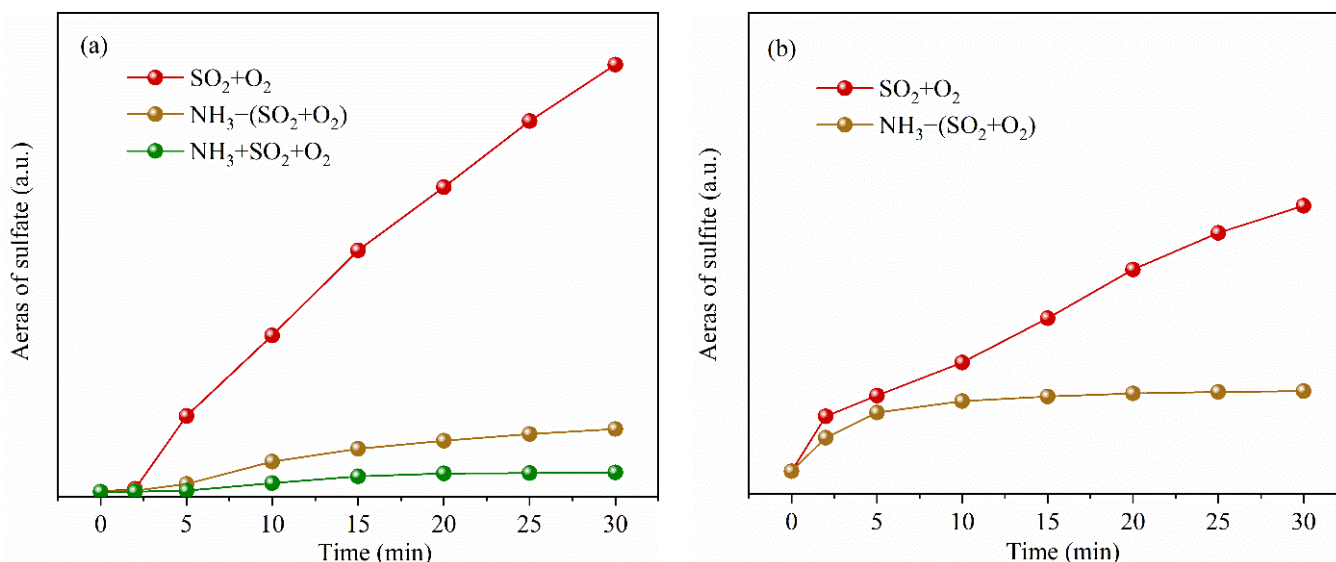


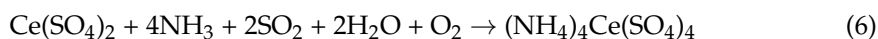
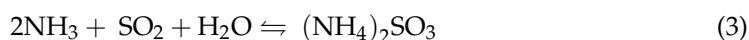
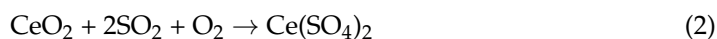
Figure 6. Evolution of (a) typical sulfate bands ($1300\text{--}1256\text{ cm}^{-1}$) and (b) sulfite band (925 cm^{-1}) as a function of time over CeNbTi catalysts that were treated with different poisoning procedures.

Significantly, the formation of sulfates/sulfites is inhibited on the NH_3 pretreated catalyst and reaches a quasi-equilibrium quickly. One possible elimination route of sulfites by ammonia is the reaction between the pre-absorbed NH_3 and sulfur dioxide to form ammonia sulfite (Equation (3)) which can decompose feasibly at much lower temperatures

(Figure S3). When NH_3 , SO_2 , and O_2 co-purge over the catalyst, almost no sulfite band is observed.

Meanwhile, the deposition amount of the sulfates decreases sharply on the NH_3 pretreated catalyst. Ammonium bisulfate is more likely to form on niobium-modified catalysts [18], which can protect ceria from sulfur poisoning. As shown by the DRIFTS result of $\text{SO}_2 + \text{O}_2$ adsorption (Figure 5c), typical signals of HSO_4^{2-} (1268 cm^{-1}) and NH_4^+ that are adsorbed on Brønsted acid sites that are provided by surface sulfates (1434 cm^{-1}) are observed. Therefore, it is reasonable that NH_4HSO_4 deposits on the pretreated catalyst according to Equation (4).

Previous studies [21,45] discovered that the decomposition of NH_4HSO_4 occurs at the temperature range of $320\text{--}450\text{ }^\circ\text{C}$ and NH_4HSO_4 can react with ceria to form ammonium cerium sulfate at lower temperatures according to Equation (5). Jangjou [14] found that the ammonia could cause the transformation from Cu_xSO_y to $(\text{NH}_4)_x\text{Cu}_y\text{SO}_z$ at $210\text{ }^\circ\text{C}$ on the Cu-SSZ-13 catalyst. Similarly, it can be seen in Figure 5b that $(\text{NH}_4)_4\text{Ce}(\text{SO}_4)_4$ species forms on the sulfated CeNbTi catalyst via Equation (6) upon NH_3 purging. Compared with $\text{Ce}(\text{SO}_4)_2$, this material can serve as an active species to a certain extent via the redox cycle between $(\text{NH}_4)_4\text{Ce}(\text{SO}_4)_4$ and $\text{NH}_4\text{Ce}(\text{SO}_4)_2$ (Figure S5). The competitive adsorption of NH_3 and SO_2 on the catalyst further reduces the surface sulfate deposition. NH_3 adsorbs preferentially on the catalyst (Figure 5d), and this preferential occupation of surface active sites by NH_3 reduces SO_x adsorption. As listed in Table 1, it can be calculated that about 4–5% of CeO_2 is deactivated by assuming $(\text{NH}_4)_4\text{Ce}(\text{SO}_4)_4$ as the distinct deposit when treating the catalyst in the $\text{SO}_2 + \text{O}_2 + \text{NH}_3 + \text{NO}$ atmosphere.



The degradation degree of CeNbTi catalyst by SO_2 poisoning under SCR conditions ($\text{NH}_3 + \text{NO} + \text{O}_2$) is much slighter than $\text{SO}_2 + \text{O}_2$ exposure alone. Based on the above results and analysis, ammonia inhibits sulfur poisoning in NH_3 -SCR to a great extent via two main ways. On the one hand, ammonia would react with sulfites and form ammonium-sulfite which can subsequently decompose. Consequently, there is much less sulfite residue on the catalyst in the presence of ammonia. On the other hand, ammonia can pre-occupy surface adsorption sites separating SO_2 and active sites to reduce the sulfation of active metal. Besides, ammonia can transform cerium sulfate to ammonium cerium sulfate with relatively higher reactivity than cerium sulfate. The corresponding SO_2 deactivation mechanisms in the presence and absence of ammonia are presented primarily in Figure 7. The present work discloses the inhibition effect of NH_3 on sulfur poisoning of CeNbTi catalyst, which provides a comprehensive mechanistic insight and enables the development of ceria-based oxide catalysts for nitrogen oxide emission control in stationary sources. It should be noted that the above findings are based on the TPD and DRIFTS results, in which the suggestion of surface species still suffers from some uncertainty and remains to be further validated.

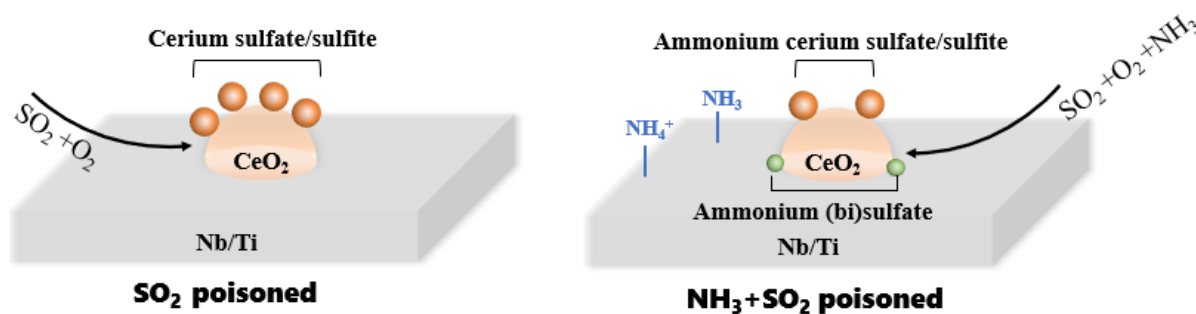


Figure 7. Schematic SO_2 deactivation mechanisms over CeNbTi in the presence and absence of NH_3 .

5. Conclusions

The deactivation of CeNbTi catalysts by exposure to SO_2 in different atmospheres was investigated. The TPD and DRIFTS techniques were employed to characterize different species that were deposited on the catalyst and investigate their formation/decomposition/transformation mechanisms. Several major conclusions were drawn as follows:

- (1) After exposure to $\text{SO}_2 + \text{O}_2$ for 6 h, the NO_x conversion at 300 °C of the catalyst decreases from almost 100% to ca. 60%, while the presence of NH_3 in the poisoning atmospheres can reserve the catalyst with about 90% NH_3 -SCR activity. Additionally, humid conditions do not result in any obvious changes in the deactivation degree of sulfur poisoning with or without NH_3 .
- (2) The types and amounts of sulfates/sulfites depend importantly on the sulfur poisoning atmospheres. When the poisoning is performed in the presence of NH_3 , the total amount of sulfites and sulfates that are deposited on the catalyst is reduced by 44% compared with that in absence of ammonia. Competitive adsorption between NH_3 and SO_2 is suggested to be one of the dominating factors for the decreased surface deposits. The pre-occupying NH_3 is confirmed to protect ceria active sites from reacting with SO_2 .
- (3) With the introduction of ammonia, not only the amounts of sulfates/sulfites decrease significantly, but also the types of sulfates change a lot from metal sulfates to ammonium sulfates. The ready decomposition behaviors of NH_4HSO_4 (and $(\text{NH}_4)_2\text{SO}_4$), as well as the transformation of cerium sulfates with more sulfate radicals that are bonded per cerium atom, can also transform to cerium ammonium sulfates which facilitate the decrease in sulfate deposits. Compared with inert metal sulfates, cerium ammonium sulfates even contribute to NH_3 -SCR reaction with the redox cycle between Ce^{3+} and Ce^{4+} in the ammonium sulfates. Additionally, metal sulfites can be partially converted into ammonium sulfite in a NH_3 -containing atmosphere which is easy to decompose even at low temperatures, resulting in fewer sulfite deposits.

Supplementary Materials: The following supporting information can be downloaded at: <https://www.mdpi.com/article/10.3390/catal12111430/s1>, Figure S1: (a) NO_x conversions and (b) N_2 selectivities of CeNbTi catalysts after the treatments in different atmospheres at 300 °C for 6 h. Reaction conditions: 500 ppm NO, 500 ppm NH_3 , 5% O_2 , 5% H_2O , N_2 in balance, and GHSV = 80,000 h^{-1} ; Figure S2: XRD patterns of (a) CeNbTi catalyst and those after poisoning in (b) $\text{SO}_2 + \text{O}_2$, (c) $\text{SO}_2 + \text{O}_2 + \text{H}_2\text{O}$ and (d) $\text{SO}_2 + \text{O}_2 + \text{NH}_3 + \text{NO} + \text{H}_2\text{O}$; Figure S3: TG and DSC curves of $(\text{NH}_4)_2\text{SO}_3$ in N_2 ; Figure S4: The outlet gas concentrations after introducing NH_3 to $\text{Ce}(\text{SO}_4)_2$ at 300 °C; Figure S5: NO_x conversion over NbTi mixed oxides and those impregnated with $(\text{NH}_4)_4\text{Ce}(\text{SO}_4)_4$, $\text{Ce}(\text{SO}_4)_2$ and $(\text{NH}_4)_2\text{SO}_3$. Reaction conditions: 500 ppm NO, 500 ppm NH_3 , 5% O_2 , 5% H_2O , N_2 in balance, and GHSV = 80,000 h^{-1} . References [46–48] are cited in supplementary materials.

Author Contributions: Conceptualization, Y.G., L.C. and X.W.; Data curation, Y.G., L.C. and Z.M.; Formal analysis, Y.G. and L.C.; Funding acquisition, X.W. and D.W.; Investigation, Y.G. and L.C.; Methodology, L.C. and X.W.; Project administration, D.W.; Resources, Z.M., D.W. and B.W.; Supervision, D.W. and B.W.; Validation, X.Z.; Writing—original draft, Y.G. and L.C.; Writing—review and

editing, Y.G., L.C., X.W., R.R. and Z.S. All authors have read and agreed to the published version of the manuscript.

Funding: The National Key R&D Program of China (No. 2017YFC0211202) and the Key Laboratory of Advanced Materials of Ministry of Education (No. 2016AML01).

Data Availability Statement: Data available upon request from the corresponding author.

Conflicts of Interest: The authors declare that they have no known competing financial interests or personal relationships that could have appeared to influence the work that was reported in this paper.

References

1. Kwon, D.W.; Park, K.H.; Ha, H.P.; Hong, S.C. The role of molybdenum on the enhanced performance and SO₂ resistance of V/Mo-Ti catalysts for NH₃-SCR. *Appl. Surf. Sci.* **2019**, *481*, 1167–1177. [[CrossRef](#)]
2. Han, L.P.; Cai, S.X.; Gao, M.; Hasegawa, J.Y.; Wang, P.L.; Zhang, J.P.; Shi, L.Y.; Zhang, D.S. Selective catalytic reduction of NO_x with NH₃ by using novel catalysts: State of the art and future prospects. *Chem. Rev.* **2019**, *119*, 10916–10976. [[CrossRef](#)]
3. Chen, L.; Si, Z.C.; Wu, X.D.; Weng, D.; Ran, R.; Yu, J. Rare earth containing catalysts for selective catalytic reduction of NO_x with ammonia: A Review. *J. Rare Earth* **2014**, *32*, 907–917. [[CrossRef](#)]
4. Mosrati, J.; Atia, H.; Eckelt, R.; Lund, H.; Agostini, G.; Bentrup, U.; Rockstroh, N.; Keller, S.; Armbruster, U.; Mhamdi, M. Nb-modified Ce/Ti oxide catalyst for the selective catalytic reduction of NO with NH₃ at low temperature. *Catalysts* **2018**, *8*, 175. [[CrossRef](#)]
5. Jiang, Y.; Bao, C.; Liu, S.; Liang, G.; Lu, M.; Lai, C.; Shi, W.; Ma, S. Enhanced activity of Nb-modified CeO₂/TiO₂ catalyst for the selective catalytic reduction of NO with NH₃. *Aerosol Air Qual. Res.* **2018**, *18*, 2121–2130. [[CrossRef](#)]
6. Liu, K.; He, H.; Yu, Y.; Yan, Z.; Yang, W.; Shan, W. Quantitative study of the NH₃-SCR pathway and the active site distribution over CeWO_x at low temperatures. *J. Catal.* **2019**, *369*, 372–381. [[CrossRef](#)]
7. Liu, J.J.; He, G.Z.; Shan, W.P.; Yu, Y.B.; Huo, Y.L.; Zhang, Y.; Wang, M.; Yu, R.; Liu, S.S.; He, H. Introducing tin to develop ternary metal oxides with excellent hydrothermal stability for NH₃ selective catalytic reduction of NO_x. *Appl. Catal. B Environ.* **2021**, *291*, 120125. [[CrossRef](#)]
8. Shan, W.P.; Yu, Y.B.; Zhang, Y.; He, G.Z.; Peng, Y.; Li, J.H.; He, H. Theory and practice of metal oxide catalyst design for the selective catalytic reduction of NO_x with NH₃. *Catal. Today* **2021**, *375*, 292–301. [[CrossRef](#)]
9. Zhang, W.; Liu, G.; Jiang, J.; Tan, Y.; Wang, Q.; Gong, C.; Shen, D.; Wu, C. Temperature sensitivity of the selective catalytic reduction (SCR) performance of Ce–TiO₂ in the presence of SO₂. *Chemosphere* **2020**, *243*, 125419. [[CrossRef](#)] [[PubMed](#)]
10. Zhang, L.; Zou, W.; Ma, K.; Cao, Y.; Xiong, Y.; Wu, S.; Tang, C.; Gao, F.; Dong, L. Sulfated temperature effects on the catalytic activity of CeO₂ in NH₃-selective catalytic reduction conditions. *J. Phys. Chem. C* **2015**, *119*, 1155–1163. [[CrossRef](#)]
11. Wijayanti, K.; Xie, K.; Kumar, A.; Kamasamudram, K.; Olsson, L. Effect of gas compositions on SO₂ poisoning over Cu/SSZ-13 used for NH₃-SCR. *Appl. Catal. B Environ.* **2017**, *219*, 142–154. [[CrossRef](#)]
12. Wijayanti, K.; Leistner, K.; Chand, S.; Kumar, A.; Kamasamudram, K.; Currier, N.W.; Yezerets, A.; Olsson, L. Deactivation of Cu-SSZ-13 by SO₂ exposure under SCR conditions. *Catal. Sci. Technol.* **2016**, *6*, 2565–2579. [[CrossRef](#)]
13. Wang, C.; Wang, J.; Wang, J.; Yu, T.; Shen, M.; Wang, W.; Li, W. The effect of sulfate species on the activity of NH₃-SCR over Cu/SAPO-34. *Appl. Catal. B Environ.* **2017**, *204*, 239–249. [[CrossRef](#)]
14. Jangjoui, Y.; Wang, D.; Kumar, A.; Li, J.; Epling, W.S. SO₂ poisoning of the NH₃-SCR reaction over Cu-SAPO-34: Effect of ammonium sulfate versus other S-containing species. *ACS Catal.* **2016**, *6*, 6612–6622. [[CrossRef](#)]
15. Wang, Y.; Yi, W.; Yu, J.; Zeng, J.; Chang, H. Novel methods for assessing the so₂ poisoning effect and thermal regeneration possibility of MO_x-WO₃/TiO₂ (M = Fe, Mn, Cu, and V) Catalysts for NH₃-SCR. *Environ. Sci. Technol.* **2020**, *54*, 12612–12620. [[CrossRef](#)] [[PubMed](#)]
16. Lian, Z.; Liu, F.; Shan, W.; He, H. Improvement of Nb doping on SO₂ resistance of VO_x/CeO₂ catalyst for the selective catalytic reduction of NO_x with NH₃. *J. Phys. Chem. C* **2017**, *121*, 7803–7809. [[CrossRef](#)]
17. An, D.; Yang, S.; Zou, W.; Sun, J.; Tan, W.; Ji, J.; Tong, Q.; Sun, C.; Li, D.; Dong, L. Unraveling the so₂ poisoning effect over the lifetime of MeO_x (Me = Ce, Fe, Mn) catalysts in low-temperature NH₃-SCR: Interaction of reaction atmosphere with surface species. *J. Phys. Chem. C* **2022**, *126*, 12168–12177. [[CrossRef](#)]
18. Ma, Y.; Cheng, S.; Wu, X.; Shi, Y.; Cao, L.; Liu, L.; Ran, R.; Si, Z.; Liu, J.; Weng, D. Low-temperature solid-state ion-exchange method for preparing Cu-SSZ-13 selective catalytic reduction catalyst. *ACS Catal.* **2019**, *8*, 6962–6973. [[CrossRef](#)]
19. Ma, Z.; Weng, D.; Wu, X.; Si, Z.; Wang, B. A novel Nb–Ce/WO_x–TiO₂ catalyst with high NH₃-SCR activity and stability. *Catal. Commun.* **2012**, *27*, 97–100. [[CrossRef](#)]
20. Song, L.; Chao, J.; Fang, Y.; He, H.; Li, J.; Qiu, W.; Zhang, G. Promotion of ceria for decomposition of ammonia bisulfate over V₂O₅-MoO₃/TiO₂ catalyst for selective catalytic reduction. *Chem. Eng. J.* **2016**, *303*, 275–281. [[CrossRef](#)]
21. Ye, D.; Qu, R.; Zheng, C.; Cen, K.; Gao, X. Mechanistic investigation of enhanced reactivity of NH₄HSO₄ and NO on Nb- and Sb-doped VW/Ti SCR catalysts. *Appl. Catal. A Gen.* **2018**, *549*, 310–319. [[CrossRef](#)]

22. Ye, D.; Qu, R.; Song, H.; Zheng, C.; Gao, X.; Luo, Z.; Ma, N.; Cen, K. Investigation of the promotion effect of WO_3 on the decomposition and reactivity of NH_4HSO_4 with NO on $\text{V}_2\text{O}_5\text{-WO}_3/\text{TiO}_2$ SCR catalysts. *RSC Adv.* **2016**, *6*, 55584–55592. [[CrossRef](#)]
23. Leistner, K.; Mihai, O.; Wijayanti, K.; Kumar, A.; Kamasamudram, K.; Currier, N.W.; Yezerets, A.L.; Olsson, L. Comparison of Cu/BEA, Cu/SSZ-13 and Cu/SAPO-34 for ammonia-SCR reactions. *Catal. Today* **2015**, *258*, 49–55. [[CrossRef](#)]
24. Udupa, M.R. Thermal decomposition of cerium (IV), cerium (III), chromium (III) and titanium (IV) sulphates. *Thermochim. Acta* **1982**, *57*, 377–381. [[CrossRef](#)]
25. Youn, S.; Song, I.; Lee, H.; Cho, S.J.; Kim, D.H. Effect of pore structure of TiO_2 on the SO_2 poisoning over $\text{V}_2\text{O}_5/\text{TiO}_2$ catalysts for selective catalytic reduction of NO_x with NH_3 . *Catal. Today* **2018**, *303*, 19–24. [[CrossRef](#)]
26. Ma, Z.; Wu, X.; Feng, Y.; Si, Z.; Weng, D.; Shi, L. Low-temperature SCR activity and SO_2 deactivation mechanism of Ce-modified $\text{V}_2\text{O}_5\text{-WO}_3/\text{TiO}_2$ catalyst. *Prog. Nat. Sci. Mater.* **2015**, *25*, 342–352. [[CrossRef](#)]
27. Li, Y.; Xiong, J.; Lin, Y.; Guo, J.; Zhu, T. Distribution of SO_2 oxidation products in the SCR of NO over $\text{V}_2\text{O}_5/\text{TiO}_2$ catalysts at different temperatures. *Ind. Eng. Chem. Res.* **2020**, *59*, 5177–5185. [[CrossRef](#)]
28. Jangjoui, Y.; Do, Q.; Gu, Y.; Lim, L.G.; Sun, H.; Wang, D.; Kumar, A.; Li, J.H.; Grabow, L.C.; Epling, W.S. Nature of Cu active centers in Cu-SSZ-13 and their responses to SO_2 exposure. *ACS Catal.* **2018**, *8*, 1325–1337. [[CrossRef](#)]
29. Shen, B.X.; Liu, T. Deactivation of $\text{MnO}_x\text{-CeO}_x/\text{ACF}$ catalysts for low-temperature $\text{NH}_3\text{-SCR}$ in the presence of SO_2 . *Acta Phys. Chim. Sin.* **2010**, *26*, 3009–3016.
30. Kwon, D.W.; Nam, K.B.; Hong, S.C. The role of ceria on the activity and SO_2 resistance of catalysts for the selective catalytic reduction of NO_x by NH_3 . *Appl. Catal. B Environ.* **2015**, *166*, 37–44. [[CrossRef](#)]
31. Qing, M.; Lei, S.; Kong, F.; Liu, L.; Zhang, W.; Wang, L.; Guo, T.; Su, S.; Hu, S.; Wang, Y.; et al. Analysis of ammonium bisulfate/sulfate generation and deposition characteristics as the by-product of SCR in coal-fired flue gas. *Fuel* **2022**, *313*, 122790. [[CrossRef](#)]
32. Liu, X.; Wang, P.; Shen, Y.; Zheng, L.; Han, L.; Deng, J.; Zhang, J.P.; Wang, A.Y.; Ren, W.; Gao, F.; et al. Boosting SO_2 -Resistant NO_x Reduction by modulating electronic interaction of short-range Fe–O coordination over $\text{Fe}_2\text{O}_3/\text{TiO}_2$ catalysts. *Environ. Sci. Technol.* **2022**, *56*, 11646–11656. [[CrossRef](#)]
33. Xu, Z.; Impeng, S.; Jia, X.; Wang, F.; Shen, Y.; Wang, P.; Zhang, D. SO_2 -Tolerant catalytic reduction of NO_x by confining active species in TiO_2 nanotubes. *Environ. Sci. Nano* **2022**, *9*, 2121. [[CrossRef](#)]
34. Jin, R.; Liu, Y.; Wang, Y.; Cen, W.; Wu, Z.; Wang, H.; Weng, X. The role of cerium in the improved SO_2 tolerance for NO reduction with NH_3 over Mn-Ce/ TiO_2 catalyst at low temperature. *Appl. Catal. B Environ.* **2014**, *148*, 582–588. [[CrossRef](#)]
35. Chang, H.; Chen, X.; Li, J.; Ma, L.; Wang, C.; Liu, C.; Schwank, J.; Hao, J. Improvement of activity and SO_2 tolerance of Sn-modified $\text{MnO}_x\text{-CeO}_2$ catalysts for $\text{NH}_3\text{-SCR}$ at low temperatures. *Environ. Sci. Technol.* **2013**, *47*, 5294–5301. [[CrossRef](#)]
36. Ye, D.; Qu, R.; Song, H.; Gao, X.; Luo, Z.; Ni, M.; Cen, K. New insights into the various decomposition and reactivity behaviors of NH_4HSO_4 with NO on $\text{V}_2\text{O}_5/\text{TiO}_2$ catalyst surfaces. *Chem. Eng. J.* **2016**, *283*, 846–854. [[CrossRef](#)]
37. Gao, F.; Tang, X.; Yi, H.; Li, J.; Zhao, S.; Wang, J.; Chu, C.; Li, C. Promotional mechanisms of activity and SO_2 tolerance of Co-or Ni-doped $\text{MnO}_x\text{-CeO}_2$ catalysts for SCR of NO_x with NH_3 at low temperature. *Chem. Eng. J.* **2017**, *317*, 20–31. [[CrossRef](#)]
38. Ma, Z.; Wu, X.; Si, Z.; Weng, D.; Ma, J.; Xu, T. Impacts of niobia loading on active sites and surface acidity in $\text{NbO}_x/\text{CeO}_2\text{-ZrO}_2$ $\text{NH}_3\text{-SCR}$ catalysts. *Appl. Catal. B Environ.* **2015**, *179*, 380–394. [[CrossRef](#)]
39. Burcham, L.J.; Datka, J.; Wachs, I.E. In situ vibrational spectroscopy studies of supported niobium oxide catalysts. *J. Phys. Chem. B.* **1999**, *103*, 6015–6024. [[CrossRef](#)]
40. Cao, L.; Chen, L.; Wu, X.; Ran, R.; Xu, T.; Chen, Z.; Weng, D. TRA and DRIFTS studies of the fast SCR reaction over $\text{CeO}_2/\text{TiO}_2$ catalyst at low temperatures. *Appl. Catal. A Gen.* **2018**, *557*, 46–54. [[CrossRef](#)]
41. Zhang, W.; Liu, G.; Jiang, J.; Tan, Y.; Wang, Q.; Gong, C.; Shen, D.; Wu, C. Sulfation effect of Ce/ TiO_2 catalyst for the selective catalytic reduction of NO_x with NH_3 : Mechanism and kinetic studies. *RSC Adv.* **2019**, *9*, 32110. [[CrossRef](#)] [[PubMed](#)]
42. Shan, W.; Liu, F.; He, H.; Shi, X.; Zhang, C. A superior Ce-W-Ti mixed oxide catalyst for the selective catalytic reduction of NO_x with NH_3 . *Appl. Catal. B Environ.* **2012**, *115*, 100–106. [[CrossRef](#)]
43. Chen, L.; Si, Z.; Wu, X.; Weng, D. DRIFT study of $\text{CuO-CeO}_2\text{-TiO}_2$ mixed oxides for NO_x reduction with NH_3 at low temperatures. *ACS Appl. Mater. Interfaces* **2014**, *6*, 8134–8145. [[CrossRef](#)] [[PubMed](#)]
44. Lonyi, F.; Valyon, J. A TPD and IR study of the surface species formed from ammonia on zeolite H-ZSM-5, H-mordenite and H-beta. *Thermochim. Acta* **2001**, *373*, 53–57. [[CrossRef](#)]
45. Tong, T.; Chen, J.; Xiong, S.; Yang, W.; Yang, Q.; Yang, L.; Li, J. Vanadium-density-dependent thermal decomposition of NH_4HSO_4 on $\text{V}_2\text{O}_5/\text{TiO}_2$ SCR catalysts. *Catal. Sci. Technol.* **2019**, *9*, 3779–3787. [[CrossRef](#)]
46. Casari, B.M.; Langer, V. Two $\text{Ce}(\text{SO}_4)_2 \cdot 4\text{H}_2\text{O}$ polymorphs: Crystal structure and thermal behavior. *J. Solid State Chem.* **2007**, *180*, 1616–1622. [[CrossRef](#)]
47. Yang, Y.; Yang, R. Study on the thermal decomposition of tetrahydrated cerie sulphate. *Thermochim. Acta* **1992**, *202*, 301–306. [[CrossRef](#)]
48. Singh Mudher, K.D.; Keskar, M.; Venugopal, V. Solid state reactions of CeO_2 , ThO_2 and PuO_2 with ammonium sulphate. *J. Nucl. Mater.* **1999**, *265*, 146–153. [[CrossRef](#)]